Received: 8 December 2022 | Revised: 12 January 2023 | Accepted: 24 January 2023

DOI: 10.1002/agt2.323

Aggregate Open Access WILEY

RESEARCH ARTICLE

Shape dependent protein-induced stabilization of gold nanoparticles: From a protein corona perspective

Special Collection: Distinguished Australian Researchers

Anastasiia Tukova[1] | **Yihan Nie**[2] | **Mohammad Tavakkoli Yaraki**[1] | **Ngoc Thanh Tran**[1] | **Jiaqiu Wang**[2,3] | **Alison Rodger**[1] | **Yuantong Gu**[2,4] | **Yuling Wang**[1]

[1]School of Natural Sciences, Faculty of Science and Engineering, Macquarie University, Sydney, New South Wales, Australia

[2]School of Mechanical, Medical and Process Engineering, Queensland University of Technology (QUT), Brisbane, Queensland, Australia

[3]Centre for Biomedical Technologies, Queensland University of Technology (QUT), Brisbane, Queensland, Australia

[4]Centre for Materials Science, Queensland University of Technology (QUT), Brisbane, Queensland, Australia

Correspondence
Yuling Wang, School of Natural Sciences, Faculty of Science and Engineering, Macquarie University, Sydney, NSW 2109, Australia.
Email: yuling.wang@mq.edu.au

Funding information
International Macquarie University Research Excellence scholarship, Grant/Award Numbers: iMQRES, Macquarie University Safety Net grant; Australian Reseach Council (ARC) Future Fellowship, Grant/Award Number: FT210100737; Early Career Researcher Grant funded by Centre for Biomedical Technologies

Abstract

Gold nanoparticles (AuNPs) are promising materials for many bioapplications. However, upon contacting with biological media, AuNPs undergo changes. The interaction with proteins results in the so-called protein corona (PC) around AuNPs, leading to the new bioidentity and optical properties. Understanding the mechanisms of PC formation and its functions can help us to utilise its benefits and avoid its drawbacks. To date, most of the previous works aimed to understand the mechanisms governing PC formation and focused on the spherical nanoparticles, although non-spherical nanoparticles are designed for a wide range of applications in biosensing. In this work, we investigated the differences in PC formation on spherical and anisotropic AuNPs (nanostars in particular) from the joint experimental (extinction spectroscopy, zeta potential and surface-enhanced Raman scattering [SERS]) and computational methods (the finite element method and molecular dynamics [MD] simulations). We discovered that protein does not fully cover the surface of anisotropic nanoparticles, leaving SERS hot-spots at the tips and high curvature edges 'available' for analyte binding (no SERS signal after pre-incubation with protein) while providing protein-induced stabilization (indicated by extinction spectroscopy) of the AuNPs by providing a protein layer around the particle's core. The findings are confirmed from our MD simulations, the adsorption energy significantly decreases with the increased radius of curvature, so that tips (adsorption energy: 2762.334 kJ/mol) would be the least preferential binding site compared to core (adsorption energy: 11819.263 kJ/mol). These observations will help the development of new nanostructures with improved sensing and targeting ability.

KEYWORDS
anisotropic gold nanoparticles, molecular dynamics simulation, protein corona, SERS, stability

1 | INTRODUCTION

Gold nanoparticle (AuNP) possesses unique optoelectronic properties, which originate from their localized surface plasmon resonance (LSPR).[1–3] LSPR is a collective oscillation of conduction electrons caused by interaction with an electromagnetic wave (light) of specific (resonant) wavelength.[3,4] The optoelectronic properties of AuNPs can be fine-tuned through colloidal chemistry, via engineering nanostructures' size and shape.[5,6] For instance, anisotropic nanoparticles such as gold nanostars and nanorods have strong extinction coefficient in the near-infrared region where light shows deeper tissue penetration whereas spherical AuNPs have distinct bright colour, that is due to light extinction in the visible region and sensitivity to change of their size.[7,8] As such, AuNPs have the potential for extensive medical applications in diagnosis and treatment. In pre-clinical settings, the use of AuNPs includes point-of-care diagnostics[9,10] (lateral flow assays such as pregnancy tests and rapid COVID-19 tests), in vivo imaging[11,12] (photoacoustic and computerised tomography), and therapeutics[13–15] (photothermal therapy, radiotherapy, catalytic therapy, and drug delivery). Although

Yihan Nie and Mohammad Tavakkoli Yaraki made equal contributions.

AuNPs treatment designs and applications are rapidly developing with some having reached clinical trials,[16–18] none has yet been approved for clinical use primarily because it is hard to predict the changes that nanoparticles undergo and how they behave in complex biological systems. Upon exposure to biological media (e.g., plasma or serum), AuNPs interact with large amounts of biomolecules which form layers around the nanoparticles. The main component of the layer is protein, and it is referred to as the protein corona (PC).[19,20] The PC characteristically consists of two layers: the 'hard corona'—a layer of tightly bound proteins attached through covalent bonds, hydrophobic and electrostatic interactions; and the 'soft corona'—a layer of loosely bound proteins outside the 'hard corona' that are attached via weak electrostatic forces. The 'soft corona' can easily be removed and thus exists in a dynamic state of constantly exchanging proteins, depending on the environment. Contrary to this, the 'hard corona' tends to remain unchanged. Even after several centrifugation-resuspension cycles, tightly bound proteins remain on the surface of nanoparticles.[19,20] The PC formation on AuNPs induces high variations in their optical properties, targeting and sensing abilities, as well as their bio-recognition by cells (caused by aggregation, morphology changes and surface fouling).[21,22] Some of the effects of a PC can also be beneficial to AuNPs applications.[23,24] Exposure of naked AuNPs to high ionic strength liquids (biological fluids like blood and urine; buffers, such as phosphate buffered saline [PBS] or isotonic saline solutions) results in their aggregation due to the ion-nanoparticle interactions and loss of electrostatic repulsion.[25,26] PC formation, however, prevents AuNPs aggregation, preserving nanoparticles stability in high ionic strength liquids thus reducing cytotoxicity, create immunological stealthiness, increasing blood-circulation time and preserving optical properties.[25]

To date, there are not many discussions on mechanisms underlying the formation of the PC on AuNPs. Majority of the studies attempting to explain AuNP-protein interaction have been carried out only on spherical particles.[25,27,28] Whilst spherical particles are often easiest to work with, it has been previously demonstrated that AuNPs with different shapes and surface roughness interact with proteins differently from spherical nanoparticles.[29–31] For example, in our previous study, we have demonstrated that ascorbate-capped gold nanostars reduce protein absorption resulting in enhanced sensing ability in protein-contained media.[32] Further, non-spherical AuNPs have been developed for a wide range of sensing applications. In order to use them with biological samples, we need to understand how anisotropic particles interact with proteins. With the increased demand for new nanostructures with enhanced optical properties, it is important to account for shape effects when considering biomedical applications. In this work, we revisit AuNP-protein interaction with different shapes of gold nanoparticles (spherical, ellipsoidal and star-shaped) and discuss possible differences in protein-induced stabilization of spherical and anisotropic nanoparticles. We utilize computational methods including finite element method (FEM) and molecular dynamics (MD) simulations to support our experimental observations. Our goal is to understand AuNP-protein interactions and the PC mechanisms of AuNPs stabilization with non-spherical particles to help create nanostructures that optimise the benefits and mitigate the flaws of PC formation.

2 | RESULTS AND DISCUSSION

2.1 | Gold nanoparticles synthesis and characterization

For this study, we prepared citrate-capped spherical and elongated gold nanoparticles of 50 and 70 nm diameter respectively (AuNP50 and AuNP70, Figure 1A,B) and ascorbate-capped gold nanostars (AuNS) of tip to tip diameter about 80 nm (Figure 1C). The synthesis methods are described in the Supporting Information (Table S1). AuNP50 and AuNP70 have distinctive LSPR bands at 531 and 551 nm, respectively. AuNS, with sharp tips (Figure S1), have a distinct LSPR peak in the near-infrared (NIR) region at 751 nm and a shoulder in the same wavelength region as the spherical nanoparticles, which is attributed to the extinction (sum of all light that is not transmitted through a sample, absorbed and scattered) mode of the AuNS core (Figure 1D). As synthesized AuNP50, AuNP70 and AuNS were monodispersed due to protective capping agents (citrate for AuNP50 and AuNP70 and ascorbate for AuNS) that preserve electrostatic repulsion between the particles (Figure 1E).

2.2 | Protein-induced stabilization of gold nanoparticles in media with high ionic strength

To test the nanoparticles' stability in high ionic strength media, AuNPs (concentration adjusted to 10^{10} particles/mL for all samples) were either centrifuged and resuspended in 1 × PBS (NaCl: 137 mM, KCl: 2.7 mM, Na_2HPO_4: 10 mM, KH_2PO_4: 1.8 mM) or incubated for 30 min with (9 mg/mL) bovine serum albumin (BSA)[32] and then centrifuged and resuspended in PBS. The presence of a large amount of salts in the PBS caused AuNPs (without protein) aggregation as indicated in the extinction spectra by a loss of peak sharpness and extinction intensity (Figure 2A–C). By way of contrast, nanoparticles coated with protein prior to resuspension in PBS, remained stable. We believe the whole serum will also be able to stabilize gold nanostructures because albumin is the major protein of serum.[25,33,34] The LSPR bands of AuNPs (with protein) remained sharp with extinction intensities similar to those of the original AuNPs. A small red-shift of the LSPR bands of AuNPs (with protein) is observed due to the change of the refractive index of the media near the nanoparticles' surface upon protein absorption.[35,36] AuNPs salt-induced aggregation or protein-induced stabilization were also confirmed by nanoparticles size analysis. The mean size and standard deviation (SD) of nanoparticles significantly increased after their resuspension in PBS due to aggregation, while after the preincubation with BSA their size did not change much, and the SD was lower compared to aggregated samples (see Supporting Information Table S1).

It is accepted that the high ionic strength medium reduces the nanoparticle citrate electrostatic repulsion leading to aggregation whereas the PC displaces the citrate but stabilizes nanoparticles by acting as a 'complex' surfactant and protecting the AuNPs.[25] That knowledge is, however, based on tests only with spherical particles. In other publications

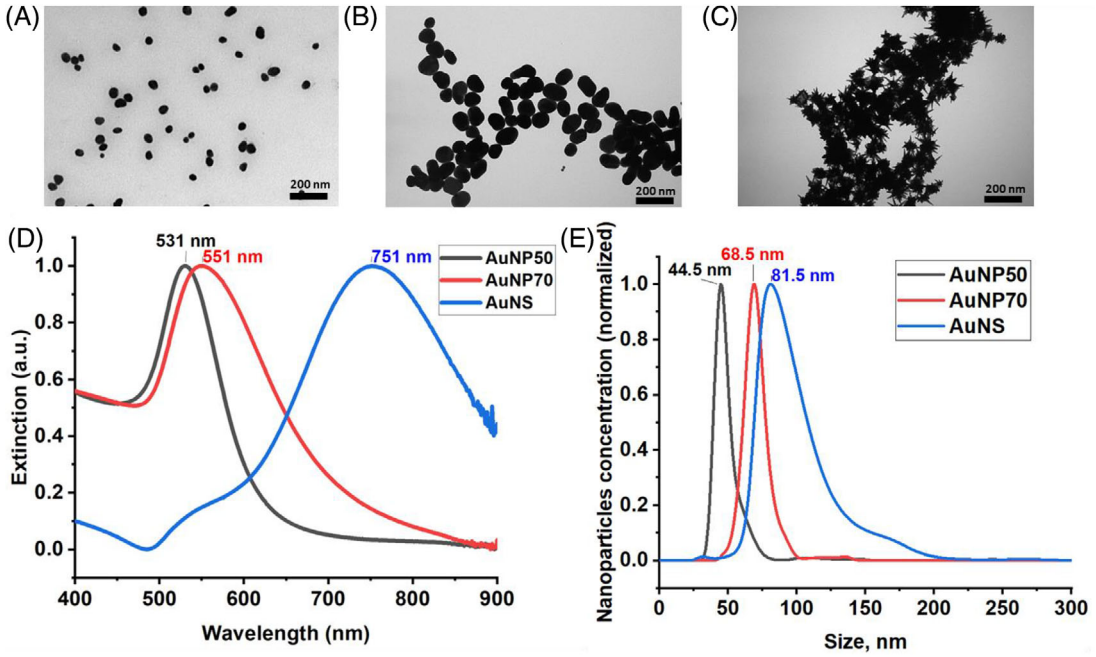

FIGURE 1 (A–C) Transmission electron microscopy images of AuNP50, AuNP70 and AuNS, respectively. (D) Extinction spectra of AuNPs normalised to 1 at their maximum. (E) Size distribution measured by nanoparticles tracking analysis (NTA)

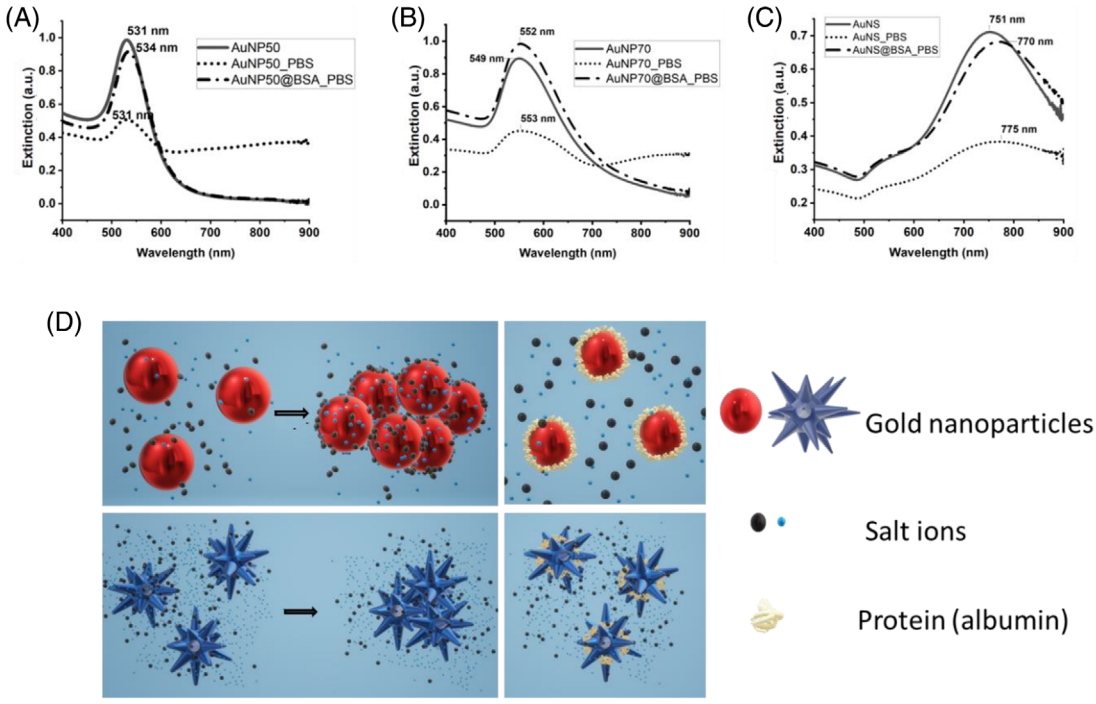

FIGURE 2 Extinction spectra of AuNPs, AuNPs in phosphate buffered saline (PBS) and AuNPs pre-treated with bovine serum albumin (BSA) prior to resuspension in PBS: (A) AuNP50, (B) AuNP70 and (C) AuNS. (D) Scheme of protein-induced stabilization of AuNPs in high ionic strength liquid

that discuss PC formation on anisotropic nanoparticles, the adsorption sites and protein-induced stabilization are either not discussed or assumed to be the same as for spherical nanoparticles—that is uniform protein coverage. However, we had previously observed that AuNS samples had reduced BSA fouling—that is, not full PC coverage—and retained the ability of AuNS to enhance Raman intensities of small molecules.[32] We, therefore, expected to see some effect of ionic strength (aggregation) even in the presence of BSA and were surprised to see the nanostar data of Figure 2, which imply that the nanostars and spherical particles behave in the same way (retaining their stability after pre-incubation with BSA). We are left with the question of how AuNPs with complex shapes have a protein-mediated stabilization mechanism, which prevents aggregation, while having plasmonic 'hot-spots', areas of high curvature with tightly confined plasmons, that create large electric filed enhancement, accessible to analytes (Figure 2D).[37]

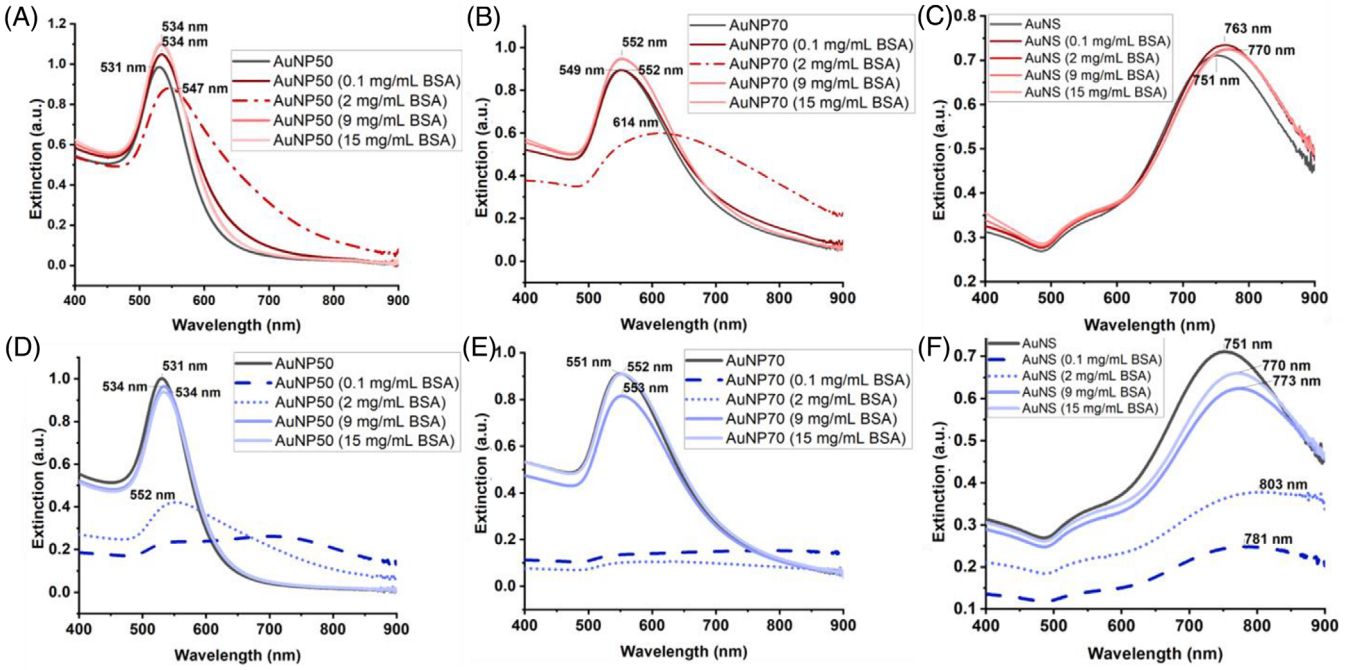

FIGURE 3 (A–C) Extinction spectra of AuNPs incubated with bovine serum albumin (BSA) without removal of unbound proteins; (D–F) Extinction spectra of AuNPs samples incubated with BSA after removal of unbound proteins (by centrifugation and resuspension)

2.2.1 | Stability as a function of protein concentration

To study further the mechanism of protein-induced stabilization of AuNPs of different shapes, we incubated AuNP50, AuNP70, and AuNS with aqueous BSA solutions of different concentrations (0.1, 2, 9 and 15 mg/mL) without any salts present. Extinction spectra of AuNPs samples incubated with BSA without removal of unbound proteins ('unwashed') are shown in Figure 3A–C. Extinction spectra of the same samples after one cycle of centrifugation and resuspension in water ('washed') are shown in Figure 3D–F. The AuNS show little change as a function of the protein concentration, but spherical particles intriguingly aggregated at intermediate protein concentrations and do not at low or high concentrations. The observed phenomenon could be attributed to the change in electrostatic repulsion between the particles, with a lower amount of protein (at concentration less than 2 mg/mL) causing little change, an intermediate amount (2–9 mg/mL) causing major disruptions, and a high amount of protein present in the solution (more than 9 mg/mL) creating favourable electrostatic-steric repulsion. [25,38,39]

After the 'washing' cycle to remove unbound proteins, all three types of AuNPs demonstrated similar behaviour patterns—at least some aggregation, when the AuNPs were preincubated with BSA at concentrations ≤2 mg/mL and stabilization, when preincubated with BSA at concentrations ≥9 mg/mL. It could be due to only very tightly bound BSA molecules remaining on the AuNPS during the 'washing', while weakly bound proteins were lost. Increasing the centrifugation-resuspension cycles will remove more proteins with consequent loss of stability due to the removal of protein layers that provide steric repulsion.[32]

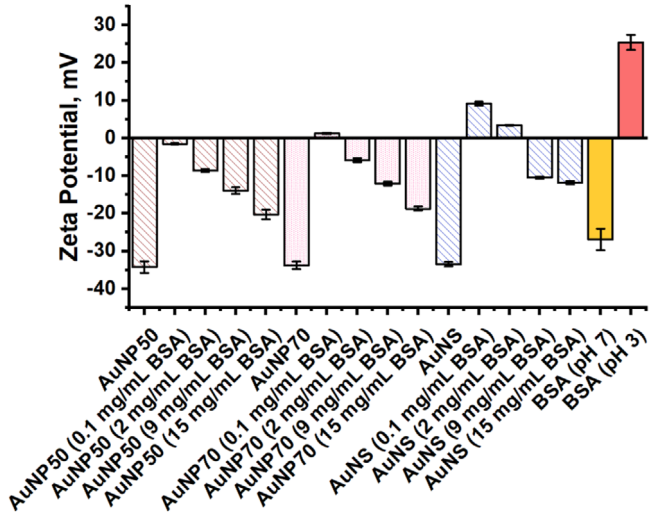

FIGURE 4 Zeta potential (surface charge) of AuNPs as prepared and of AuNPs incubated with bovine serum albumin (BSA) after removal of unbound proteins and resuspended in water

These observations are supported by zeta potential measurements of the 'washed' samples (Figure 4). Aqueous-media exposed –COOH groups of the capping agents are ionized, creating negative surface charges and an acidic pH of the colloid AuNPs solutions (pH ∼ 3 for all three solutions after synthesis).[40] At a pH lower than its isoelectric point, BSA molecules have a net positive charge. Thus, after preincubation with a low concentration of BSA and removal of any unbound protein, the absolute surface charge of the AuNPs@BSA nanoparticles is much lower than the as-synthesized samples—almost neutral causing aggregation due to the reduction of interparticle electrostatic repulsion. We speculate that with the increase of protein bound to the nanoparticles, the solution pH increases, and

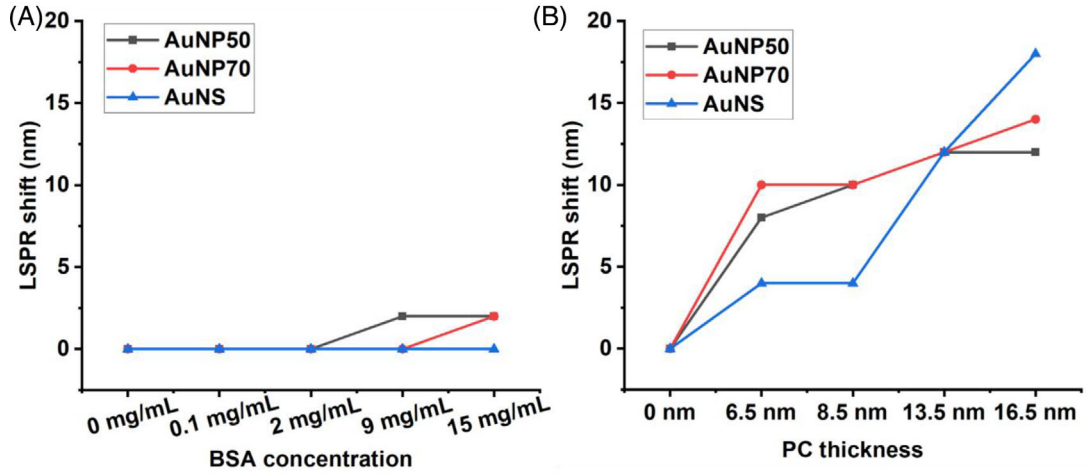

FIGURE 5 Finite element method (FEM) simulated localized surface plasmon resonance (LSPR) peak shift with the change of (A) protein concentration in the solution and (B) protein corona thickness around nanoparticles (for AuNS the PC is designed around the core only)

AuNPs@BSA charge stabilizes at around—15 mV. It is generally accepted that absolute values of surface charge lower than 30 mV are not high enough to prevent NPs from aggregation due to a lack of electrostatic repulsion.[41,42] However, the stability of the AuNPs@BSA particles is enhanced by the BSA layer, presumably by its steric repulsion.

To understand the differences in the LSPR peak shift and influence of adsorbed and free BSA molecules on the extinction of AuNPs we performed FEM simulations of extinction spectra of AuNP50, AuNP70 and AuNS, with different BSA concentrations (unbound proteins) and with different thicknesses of PC around them (bound proteins) (see Supporting Information for more details). The approximate thickness of PC was calculated by evaluating the size of AuNP50 and AuNS70 before and after incubation with BSA (estimated to be about ~6.5 nm see Supporting Information Table S1). The thickness of the PC around the core of the AuNS was theoretically estimated based on dimensions of BSA obtained from the RCSB PDB (Research Collaboratory for Structural Bioinformatics Protein Data Bank) database and the average size of the core of the AuNS, excluding the spikes protrusions. According to the simulation results, the LSPR peak position is not affected much by the presence of free protein in the solution, while the thickness of PC has a significant impact, creating a larger red shift with the increase of its thickness (Figure 5).

Based on the experimental (Figure 3A–C) and simulation results, the PC on spherical and anisotropic nanoparticles seems to form quite differently. The PC on spherical and ellipsoidal nanoparticles (AuNP50 and AuNP70) forms quickly (estimated to be less than 2 min) [43,44] and reaches a certain thickness about ~6.5 nm (see Supporting Information Table S1) with 9 mg/mL concentration of BSA after which further increase of protein amount does not contribute to the hard BSA-layer formation.[45] However, the LSPR shift of AuNS is more pronounced and changes with the increase of protein concentration in the media, which indicates an increase of the PC thickness. The thickness change was estimated by assuming that the PC forms around the full surface of spherical nanoparticles, so its thickness can be deduced from nanoparticle size. Build-up of PC leads to a red-shift in the AuNP extinction spectra (due to change of refractive index near the surface). The thickness of PC around AuNS cannot be evaluated with size analysis. We also could not evaluated PC thickness via cryo-transmission electron microscopy (TEM) in our previous work,[32] as the PC does not form uniformly over the surface of the AuNS. Instead, the hard corona presence was confirmed with the red-shift in extinction spectra, confirmed by both experimental and simulation data.

2.3 | Protein interaction with spherical and anisotropic nanoparticles

Surface-enhanced Raman spectroscopy (SERS) signal by AuNPs requires close proximity (up to 5 nm) between the analyte and the particle surface,[46,47] preferably near 'hot spots'. We, therefore, used SERS measurements to confirm the BSA adsorption onto the AuNP50 and AuNP70. As can be seen from Figure 6A,B, there are multiple high intensity peaks in the SERS spectra of spherical particles incubated with BSA (see Supporting Information Table S2 for peaks assignment). By way of contrast, the SERS spectrum of AuNS incubated with BSA (Figure 6C) does not have any distinct peaks above the noise level. We know from the extinction spectroscopy and zeta potential analysis given above that the protein does adsorb on the AuNS particles, but it seems that nanoparticles 'hot-spots' are protein-free.

To explain the observed SERS results, the electric field distribution around the AuNS was simulated via FEM calculation (Figure 7A). The electric field around tips has a dramatic enhancement compared to the region around the core so protein molecules, adsorbed onto the core would not have a significant SERS enhancement, although they do contribute to the redshift of the LSPR (Figure 7B). Spherical nanoparticles do not have areas with high curvature, which makes enhancement homogeneous on the surface and much weaker, compared to AuNS 'hot-spots' enhancement (Supporting Information Figure S2).

To further study this phenomenon, we performed MD simulations to reveal the potential link between gold surface curvature (shape of AuNPs) and the adsorption of BSA protein.

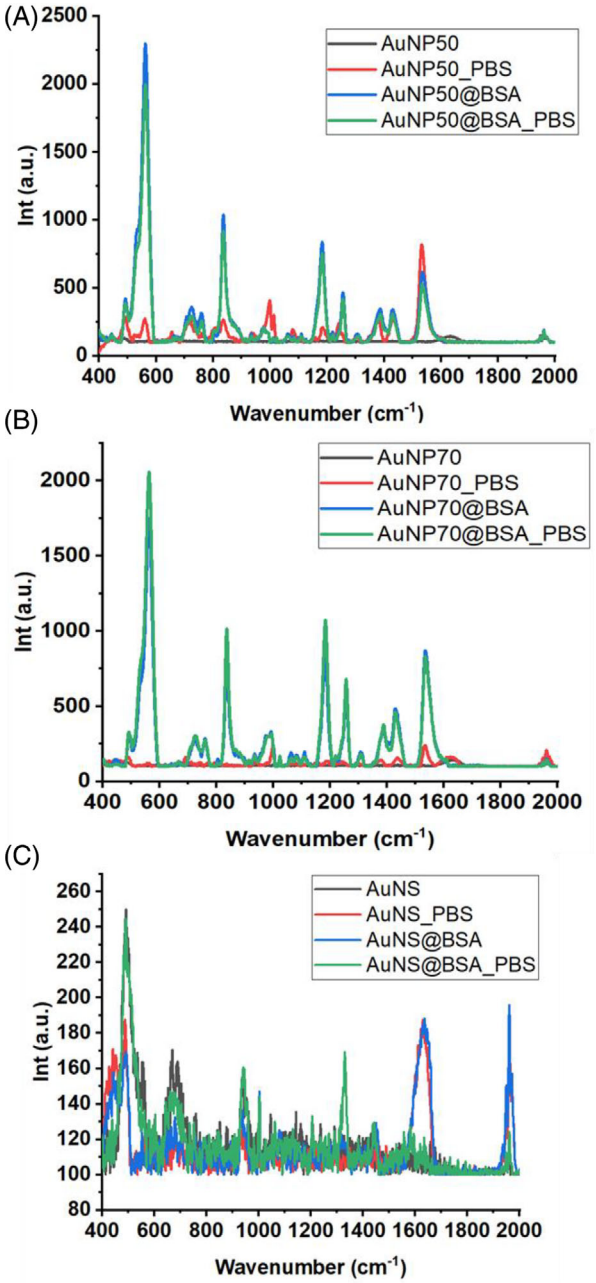

FIGURE 6 Surface-enhanced Raman scattering (SERS) spectra of AuNPs, AuNPs in phosphate buffered saline (PBS), AuNPs incubated with 9 mg/mL bovine serum albumin (BSA) and AuNPs preincubated with 9 mg/mL BSA and resuspended in PBS: (A) AuNP50, (B) AuNP70 and (C) AuNS.

Four types of gold surface models were constructed (Figure 8A–D): plane (P), truncated cone large, truncated cone small, and spherical tip. For other details regarding the simulation please see Supporting Information. Initially, the protein was placed away from the gold surface with a minimum distance of 0.8 nm. The protein was adsorbed on the gold surface within a 1 ns simulation. The energy of the system was averaged over a 1 ns simulation after adsorption under a canonical ensemble. The temperature was set to be 300 K. To quantify the adsorption strength between BSA and the gold surface, the adsorption energy E_{ad} was calculated as (Equation 1):

$$E_{\mathrm{ad}} = -\left(E_{\mathrm{Gold@BSA}} - E_{\mathrm{BSA}} - E_{\mathrm{Gold}}\right), \qquad (1)$$

where $E_{\mathrm{Gold\&BSA}}$, E_{BSA} and E_{Gold} are energies of Gold@BSA, BSA and gold surface structures respectively. A larger adsorption energy indicates a stronger interaction between BSA and the gold surface, so the BSA is more likely to remain adsorbed and less likely to desorb under the local thermal fluctuations.[48] For each gold surface model, the extreme and average adsorption energies along 10 directions are presented in Figure 8E. The complete results including each orientation can be found in the Supporting Information Table S3. When the curvature of the gold surface increases, the number of gold atoms within the force cut-off distance of BSA decreases, and the van der Waals force decreases. Thus, with the increase of the radius of curvature, the adsorption energy decreases significantly. Such results illustrate that BSA is less likely to be adsorbed on the surface with large curvatures, such as the spikes on the gold nano star surface, which supports the experimental finding that BSA is seldom found on the AuNS tips.

The adsorbed amino acids, as defined by being less than 0.5 nm from the gold surface, were also counted. For the same type of gold surface, the adsorbed amino acid number had a positive correlation with the adsorption energy (Supporting Information Table S3). However, for different surfaces, the average adsorbed amino acid number is similar, but the adsorption energy per amino acid for the smaller curvature surfaces is significantly higher. The types of the adsorbed amino acids were counted, and the results are shown in Supporting Information Figure S3.

3 | CONCLUSION

In this work, we have studied AuNP-protein interactions and found some notable differences between BSA adsorption to spherical and anisotropic (star-shaped) nanoparticles. In particular, we have considered the effects of high ionic strength salt and varying protein concentrations (as represented by the main protein in most biological media, BSA). We found salt and proteins stabilise or destabilise the particles depending on their concentrations and the particle shape. The protein layers strongly adsorbed onto the AuNPs surfaces, also known as the hard PC, affect their biological identity and alter their function and properties. We have found that the PC is not always the 'enemy'. Formation of protein layers around nanoparticles can increase their stability in the presence of salts. To utilize the benefits and avoid the drawbacks of PC formation requires a thorough understanding of nanoparticle-protein interaction patterns. For spherical nanoparticles, the PC formation was confirmed by extinction spectroscopy, zeta potential and SERS measurements. However, in the case of anisotropic nanostars while extinction spectroscopy and zeta potential analysis indicated the presence of a PC, there was no significant protein SERS enhancement. We deduced that this meant the proteins do not bind to the sites on the nanostars which generate the strongest SERS enhancement. With FEM simulations we have shown that the electric field enhancement around different parts of nanostars varies, with the strongest enhancement at the tips and almost no enhancement at the core. MD simulations, conversely, showed more proteins would bind near the more planar core of the nanostars than at the tips. Thus, we see evidence of a PC on nanostars but the SERS binding sites remain available to

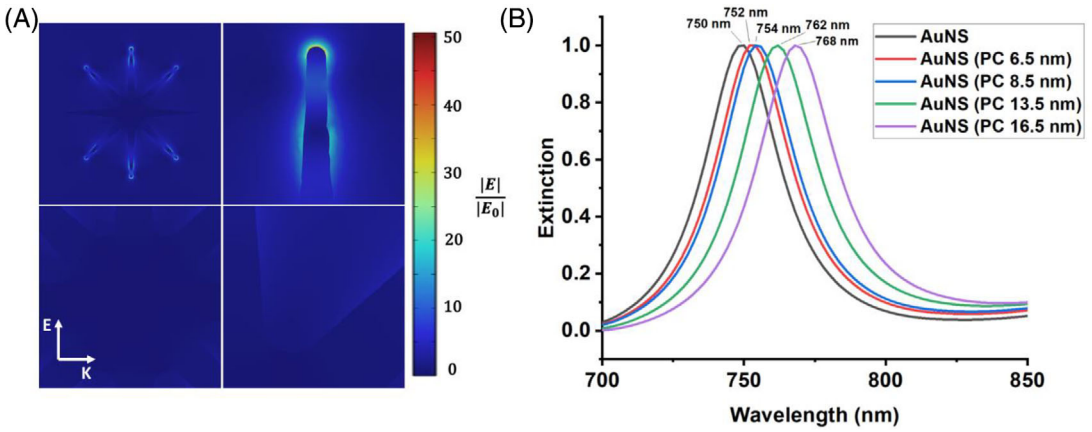

FIGURE 7 (A) The simulated enhanced electric field distribution near the tips (top row) and around the core (bottom row) of AuNS. E is the polarisation direction, and K is the propagation direction. The wavelength of the incident light is 785 nm. (B) The simulated localized surface plasmon resonance (LSPR) peaks of AuNS@BSA with different thicknesses of protein layers around the core (PC – protein corona and its thickness).

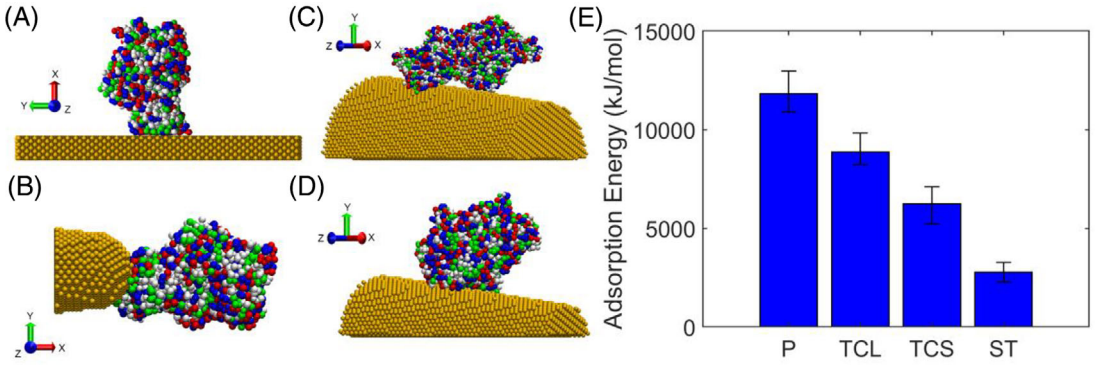

FIGURE 8 The adsorption configurations of the maximum adsorption energy for (A) the P (plane) model; (B) the spherical tip (ST) model (0_270_0 bovine serum albumin [BSA] orientation); (C) the truncated cone large (TCL) model (0_180_0 BSA orientation); (D) the truncated cone small (TCS) model (90_0_0 BSA orientation). (E) The average adsorption energy for each model. The error bar shows the maximum and the minimum value in 10 orientations.

detect other analytes. Overall, this fascinating result means that anisotropic nanoparticles might enjoy protein-mediated stabilization and other benefits of PC, while having their plasmonic properties preserved for small molecule analytes to bind to their 'hot-spots', which are free from protein binding.

ACKNOWLEDGMENTS

A.T. acknowledges funding support from the International Macquarie University Research Excellence scholarship (iMQRES). A.R and Y.W acknowledge the funding support from Macquarie University Safety Net grant. Y.W acknowledges funding support from Australian Reseach Council (ARC) via Discovery Projects (DP200102004) and Future Fellowship (FT210100737). J.W. would like to acknowledge the financial support from the Early Career Researcher Grant funded by Centre for Biomedical Technologies, Queensland University of Technology (QUT). The High-Performance Computing (HPC) resources provided by QUT are gratefully acknowledged (Y.N.). The authors would like to acknowledge Prof. Liangzhi Kou (QUT) contribution in enabling collaboration and advice on conducted work.

CONFLICT OF INTEREST STATEMENT

The authors declare no conflicts of interest.

DATA AVAILABILITY STATEMENT

The data that support the findings of this study are available from the corresponding author upon reasonable request.

ORCID

Anastasiia Tukova https://orcid.org/0000-0003-0316-1814
Mohammad Tavakkoli Yaraki https://orcid.org/0000-0002-6987-7885
Jiaqiu Wang https://orcid.org/0000-0001-7710-3508
Yuling Wang https://orcid.org/0000-0003-3627-7397

REFERENCES

1. H. Bin Jeon, P. V. Tsalu, J. W. Ha, *Sci. Rep.* **2019**, *9*, 13635.
2. J. Jana, M. Ganguly, T. Pal, *RSC Adv.* **2016**, *6*, 86174.
3. L. Wang, M. Hasanzadeh Kafshgari, M. Meunier, *Adv. Funct. Mater.* **2020**, *30*, 2005400.
4. M. Tavakkoli Yaraki, A. Tukova, Y. Wang, *Nanoscale* **2022**, *14*, 15242.
5. Y. A. Attia, D. Buceta, F. G. Requejo, L. J. Giovanetti, M. A. López-Quintela, *Nanoscale* **2015**, *7*, 11273.
6. S. He, M. W. C. Kang, F. J. Khan, E. K. M. Tan, M. A. Reyes, J. C. Y. Kah, *J. Opt.* **2015**, *17*, 114013.
7. P. Chapagain, G. Guisbiers, M. Kusper, L. D. Geoffrion, M. Benamara, A. Golden, A. Bachri, L. Hewavitharana, *ACS Omega* **2021**, *6*, 6871.
8. X.-L. Liu, J.-H. Wang, S. Liang, D.-J. Yang, F. Nan, S.-J. Ding, L. Zhou, Z.-H. Hao, Q.-Q. Wang, *J. Phys. Chem. C* **2014**, *118*, 9659.

9. S. Khizar, A. Elaissari, A. A. Al-Dossary, N. Zine, N. Jaffrezic-Renault, A. Errachid, *Curr. Top. Med. Chem.* **2022**, *22*, 807.
10. R. W. Lei, D. Wang, H. Arain, C. Mohan, *Diagnostics* **2022**, *12*, 1107.
11. B. B. Oliveira, D. Ferreira, A. R. Fernandes, P. V. Baptista, *WIREs Nanomed. Nanobiotech.* **2023**, *15*, 1836.
12. R. S. Devi, A. Girigoswami, M. Siddharth, K. Girigoswami, *Appl. Biochem. Biotechnol.* **2022**, *9*, 4187.
13. Y. Chen, X. Feng, *Int. J. Pharm.* **2022**, *625*, 122122.
14. A. Veeren, M. O. Ogunyankin, J. E. Shin, J. A. Zasadzinski, *Pharmaceutics* **2022**, *14*, 701.
15. F. Sauvage, V. P. Nguyen, Y. X. Li, A. Harizaj, J. Sebag, D. Roels, V. Van Havere, K. Peynshaert, R. H. Xiong, J. C. Fraire, M. J. Tassignon, K. Remaut, Y. M. Paulus, K. Braeckmans, S. C. De Smedt, *Nat. Nanotechnol.* **2022**, *17*, 552.
16. R. Zhang, F. Kiessling, T. Lammers, R. M. Pallares, *Drug Deliv. Transl. Res.* **2023**, *13*, 378.
17. A. N. DuRoss, J. Phan, A. J. Lazar, J. M. Walker, A. R. Guimaraes, C. Baas, S. Krishnan, C. R. Thomas, C. R. Sun, A. F. Bagley, *Interdiscip. Rev. nanobiotechnology* **2022**, 1867.
18. Y. Yang, X. Zheng, L. Chen, X. F. Gong, H. Yang, X. M. Duan, Y. X. Zhu, *Int. J. Nanomed.* **2022**, *17*, 2041.
19. T. Kopac, *Int. J. Biol. Macromol.* **2021**, *169*, 290.
20. R. Cai, C. Chen, *Adv. Mater.* **2019**, *31*, 1805740.
21. X. Wang, W. Zhang, *J. Control. Release* **2022**, *345*, 832.
22. Q. Xiao, M. Zoulikha, M. Qiu, C. Teng, C. Lin, X. Li, M. A. Sallam, Q. Xu, W. He, *Adv. Drug Deliv. Rev.* **2022**, *186*, 114356.
23. E. L. L. Yeo, N. 'Ain Azman, J. C. Y. Kah, *Langmuir* **2021**, *37*, 4913.
24. N. Habibi, A. Mauser, Y. Ko, J. Lahann, *Adv. Sci.* **2022**, *9*, 2104012.
25. J. Piella, N. G. Bastús, V. Puntes, *Bioconjug. Chem.* **2017**, *28*, 88.
26. D. Huang, H. Zhou, H. Liu, J. Gao, *Dalt. Trans.* **2015**, *44*, 17911.
27. M. N. Hossen, C. K. Elechalawar, V. Sjoelund, K. Moore, R. Mannel, R. Bhattacharya, P. Mukherjee, *Cancer Nanotechnol*. **2021**, *12*, 1.
28. M. S. Jahan Sajib, P. Sarker, Y. Wei, X. Tao, T. Wei, *Langmuir* **2020**, *36*, 13356.
29. R. Lopes Rodrigues, F. Xie, A. E. Porter, M. P. Ryan, *Nanoscale Adv*. **2020**, *2*, 1144.
30. T. Bewersdorff, E. A. Glitscher, J. Bergueiro, M. Eravci, E. Miceli, A. Haase, M. Calderón, *Mater. Sci. Eng. C* **2020**, *117*, 111270.
31. S. Dominguez-Medina, L. Kisley, L. J. Tauzin, A. Hoggard, B. Shuang, A. S. D. S. Indrasekara, S. Chen, L.-Y. Wang, P. J. Derry, A. Liopo, E. R. Zubarev, C. F. Landes, S. Link, *ACS Nano* **2016**, *10*, 2103.
32. A. Tukova, I. C. Kuschnerus, A. Garcia-Bennett, Y. Wang, A. Rodger, *Nanomaterials* **2021**, *11*, 2565.
33. N. Ajdari, C. Vyas, S. L. Bogan, B. A. Lwaleed, B. G. Cousins, *Nanomed. Nanotechnol. Biol. Med.* **2017**, *13*, 1531.
34. J. Wang, W. Anderson, J. Li, L. L. Lin, Y. Wang, M. Trau, *J. Colloid Interface Sci.* **2019**, *537*, 536.
35. S. Kaur, N. K. Bari, S. Sinha, *Amino Acids* **2022**, *54*, 441.
36. S. Szunerits, J. Spadavecchia, R. Boukherroub, *Rev. Anal. Chem.* **2014**, *33*, 153.
37. D. Radziuk, H. Moehwald, *Phys. Chem. Chem. Phys.* **2015**, *17*, 21072.
38. C. Vasti, D. A. Bedoya, R. Rojas, C. E. Giacomelli, *J. Mater. Chem. B* **2016**, *4*, 2008.
39. K. Mishra, P. K. Das, *Phys. Chem. Chem. Phys.* **2019**, *21*, 7675.
40. M. Benelmekki, *Nanomaterials*, Morgan & Claypool Publishers, Kentfield, CA, **2019**.
41. N. Raval, R. Maheshwari, D. Kalyane, S. R. Youngren-Ortiz, M. B. Chougule, R. K. Tekade, *Adv. Pharm. Prod. Dev. Res.* Ch.10, **2019**, 369.
42. M. K. Rasmussen, J. N. Pedersen, R. Marie, *Nat. Commun.* **2020**, *11*, 2337.
43. V. H. Nguyen, B.-J. Lee, *Int. J. Nanomed.* **2017**, *12*, 3137.
44. E. Casals, T. Pfaller, A. Duschl, G. J. Oostingh, V. Puntes, *ACS Nano* **2010**, *4*, 3623.
45. R. García-Álvarez, M. Vallet-Regí, *Nanomaterials* **2021**, *11*, 888.
46. A. I. Pérez-Jiménez, D. Lyu, Z. Lu, G. Liu, B. Ren, *Chem. Sci.* **2020**, *11*, 4563.
47. G. Kumari, J. Kandula, C. Narayana, *J. Phys. Chem. C* **2015**, *119*, 20057.
48. Z. He, J. Zhou, *Carbon N. Y.* **2014**, *78*, 500.

SUPPORTING INFORMATION

Additional supporting information can be found online in the Supporting Information section at the end of this article.

How to cite this article: A. Tukova, Y. Nie, M. Tavakkoli Yaraki, N. T. Tran, J. Wang, A. Rodger, Y. Gu, Y. Wang, *Aggregate* **2023**, *4,* e323. https://doi.org/10.1002/agt2.323